

Investigation and Application of High Megavoltage X-Ray Imaging Mode in Radiotherapy

Quanshi Zhang, Xiwen Wang, Qiyin Sun, Yuehui Jin, Yun Li, Ziyu Li, Tao Sun, Liang Wang

The Cancer Affiliated Hospital of Soochow University American Fox Chase Wuxi Cancer Center, Wuxi, China
Email: zqs1962@aliyun.com

Received 28 October 2015; accepted 14 February 2016; published 17 February 2016

Copyright © 2016 by authors and Scientific Research Publishing Inc.

This work is licensed under the Creative Commons Attribution International License (CC BY).

<http://creativecommons.org/licenses/by/4.0/>



Open Access

Abstract

After drawbacks and shortages of using conventional kV or MV imaging mode were analyzed, this study proposes a new position verification mode with using the energy larger than 15 MeV or nominal accelerating potential greater than 25 MV X-Ray. The new position verification mode is named HMV imaging mode. Along with the comparison of theoretical analyses, phantom experiments and clinical results to the original imaging modes, this report is going to demonstrate the HMV imaging mode is superior to traditional kV and MV imaging modes. This report first theoretically analyzed three main effects of X-ray interacting with medium by numerous equations and compared their mass attenuation coefficient with different types of tissue. X-ray irradiated on a "Catphan 500" cylinder phantom with different energies to verify these theoretical results. Furthermore, based on phantom experiments' results, we have done numerous clinical trials and comparisons with patient's clinical results. The theoretical and experimental results illustrate that the scanned images from HMV mode have a good quality and have ability to identify different tissue components clearly. HMV imaging mode overcomes drawbacks of position verification from both kV and MV level imaging mode as well as keeping advantages of kV and MV imaging mode. The result indicates that HMV is a good position verification mode in radiotherapy.

Keywords

High Energy X-Ray, X-Ray Imaging Mode, Position Verification, Reaction Cross-Section

1. Introduction

In today's world, choosing reasonable ways to detect and treat malignant tumor becomes a hot debated issue

because tumors may threaten human life. Radiotherapy is one of the three significant therapy strategies for the cancer treatment. Now, the radiotherapy has entered new era of accurate treatment with applying 3D conformal and Intensity-modulated therapy (IMRT) [1] [2]. Chen [3] stated tumor's verification image during radiotherapy period is an essential process and Imaging Guide Radiotherapy Therapy (IGRT) is a new developed system for ensuring tumor to be irradiated at precise position. Currently, kV level imaging mode (kV) and MV level imaging mode (MV) imaging modes are two main X-ray imaging modes for IGRT on linear accelerators for radiation therapy [4] [5]. Their X-ray energy ranges from 60 kV to 120 kV and 4MV to 15 MV respectively. However, both of these modes have unavoidable shortcoming and inadequate.

For radiotherapy equipments with kV level imaging mode, it has good image quality and contrast between tissues and anatomical structures. However, the kV imaging mode needs to equip a set of additional kV X-ray generators and bound up with control sections (**Figure 1(a)**) [6]. These functions not only increase cost of additional control sections and raise unsafe factors during treatment process, but also heighten failure rates of the whole system and increase the system potential failure rate. The main issues of kV imaging mode are additional radiation dose delivered to patients during the guidance period and the acquired guidance images from this mode have different isocenter from the treatment beam [7].

For radiotherapy equipments with MV level imaging mode, which a Electronic Portal Imaging Device (EPID) mounted on the opposite of the radiation source [8], do not have shortcomings and the insufficiency as in kV level imaging mode because MV imaging mode uses the same X-ray source for treatment and imaging (**Figure 1(b)**). The on-board MV level-imaging mode does not increase the cost and unsafe factors, but is easy to correct additional dosage that is introduced from verification imaging. Additionally, along with relative algorithms, dose-guided Radiotherapy (DGRT) is able to use with MV level CBCT. When a metal implanted into human, artifacts that produced from MV CBCT is much smaller than it generated from kV CBCT. Based on these issues, MV level imaging mode would be an ideal mode for IGRT. However, resolving capability contrast between tissues and anatomical structures is not that good as the images acquired from kV level imaging mode. This is a fatal flaw of the MV mode and easily leads to larger position errors and uncertainty.

Currently, many manufacturers invest more employees, extend material resources and researchers with applying additional software or equipment modifications to improve the image resolving capability and quality for MV level imaging mode. Such plans of redesigning the size of EPID in MV imaging mode aim to collect more photons, combining kV imaging with optical imaging devices minimizing dose on patients [7] and using a dual energy radiotherapy imager to acquire the scanning images from both kV and MV imaging mode [9]. However, there were not effective methods that can significantly improve the image contrast and quality. This was mainly because Compton Effect within the range of 4 MV to 15 MV X-ray interacting with medium is independent of the atomic number of medium and the energy of photon. Therefore, many manufacturers (*i.e.* Elekta and Varian [9] and Siemens [10]) are forced to use both MV level imaging mode and kV level imaging mode in one Linac system (**Figure 1(c)**).

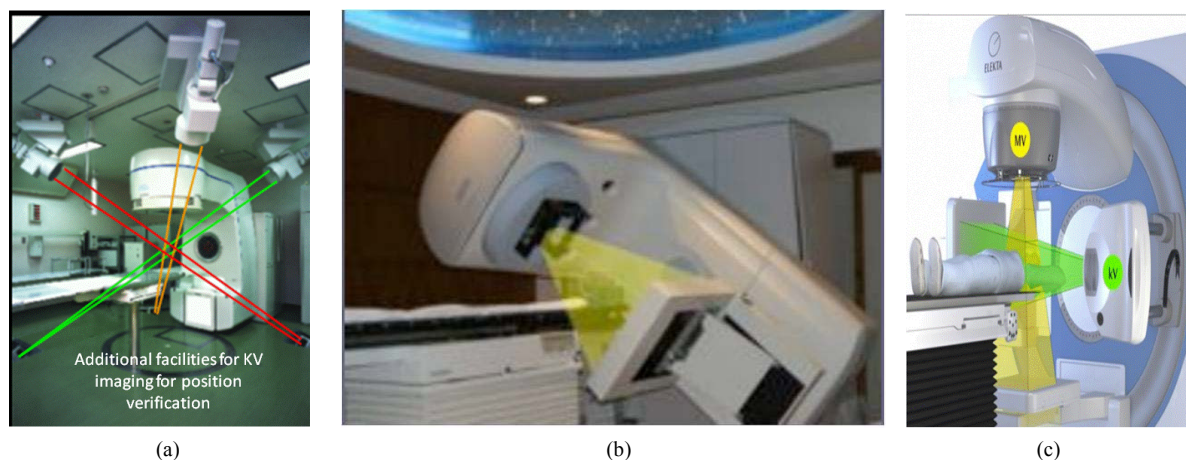


Figure 1. (a) kV imaging mode acquired with three additional X-ray generators installed on the roof with different angles. (b) MV imaging mode acquired from the EPID below nozzle. (c) Additional facility for kV imaging mode mounted on gantry and MV imaging mode from the bottom-imaging detector.

Our study proposes a high megavoltage-imaging mode (HMV mode) for IGRT. In the HMV mode, X-ray photon energy is bigger than 15 MeV, or nominal acceleration potential is greater than 25 MV. The HMV mode improves the contrast and quality of imaging as well as not requires additional X-ray generator and control parts as being used in the kV imaging mode. Therefore, the HMV mode is possible to preserve all of benefits of kV and MV modes as well as remove the obstacles of size, cost and complexity of kV mode.

2. Materials and Methods

2.1. Theoretical Basis and Method

The basic principle of X-ray imaging is the amount of efficient energy that deposited or absorbed in the medium. The more deposited or absorbed energy, the better quality of images will be. The larger differences of the absorbed or deposited energy, the higher capability distinguish these tissues. In other words, it is easier to identify and distinguish the tissue component.

There are three basic forms of the X-ray or photon interacting with mediums. The first one called Photoelectric Effect (PE), which the photon energy is generally lower than 200 keV. The second one is Compton Effects (CE), which the photon energy is about 0.2 - 5.0 MeV and the last one named Electronic Pair Effect (EPE), which the photon energy is larger than 5.0 MeV.

The reaction cross-section σ , in cm^{-2} , is the parameter describes area of the reaction probability for X-ray interacting with medium or matter. The larger cross-section, the more effective energy can be deposited or absorbed in imaging detector, therefore the more benefit to the quality of image.

Equations among the cross-section σ , the atomic number Z of the matter and the X-ray energy ($h\nu$) describe below.

2.1.1. Theoretical Basis and Method

$$\sigma_t = \frac{z^n}{(h\nu)^3} \quad (1)$$

where σ is the cross-section, the subscript τ represents Photoelectric Effect. The parameter z is atomic number, n ranges from 3 to 4 and $h\nu$ is the energy of photon. The PE is a dominant reaction for kV imaging mode. From this equation, when X-ray interacting with medium, the reaction cross-section is inversely proportional to the cubic of the photon energy ($h\nu$). The smaller of the photon energy and the larger atomic number of medium both lead to the larger scale of the cross-section, and therefore the better of the image quality will be.

2.1.2. Cross-Section for the Compton Effect

$$\begin{aligned} e^\sigma &= 2\pi \int_0^\pi \frac{de^\sigma}{d\Omega_\theta} \sin\theta d\theta \\ &= 2\pi r_e^2 \left\{ \frac{1+\alpha}{\alpha^2} \left[\frac{2(1+\alpha)}{1+2\alpha} - \frac{\ln(1+2\alpha)}{\alpha} \right] + \frac{\ln(1+2\alpha)}{2\alpha} - \frac{1+3\alpha}{(1+2\alpha)^2} \right\} \end{aligned} \quad (2)$$

where α is the ratio between the incident X-ray energy ($h\nu$) and electron static energy ($m_e c^2$) which equal 0.511 MeV. Parameter θ is scattering angle of the scattered photons. r_e is a classical radius of the electron. From Equation (2), the cross-section of CE is independent of the atomic number of medium and the energy of X-ray or photon.

2.1.3. Cross-Section for the Electronic Pair Effect

$$\text{While } h\nu > 2m_e c^2, \sigma_p \propto Zh\nu \quad (3)$$

$$\text{While } h\nu \gg 2m_e c^2, \sigma_p \propto Z^2 \ln(h\nu) \quad (4)$$

where $h\nu$ represents the energy of X-ray, $m_e c^2$ is the electronic static energy, σ_p is cross-section of EPE, Z is the atomic number of the medium. From Equations (3) and (4), the more irradiate X-ray's energy and the bigger scale

of the cross-section both lead to the better quality of images.

In practical work, we commonly use mass attenuation coefficient (μ/ρ) rather than the cross-section σ with the units of m^2/kg or cm^2/g to describe the probability of X-ray photon interacts with medium in unit thickness. The subscript p represents the effect of EPE. The equation between μ_p/ρ and the medium cross-section σ is:

$$\frac{\mu_p}{\rho} = \frac{N_A}{M_A} \sigma_p \quad (5)$$

In which, μ_p/ρ is the mass attenuation coefficient of X-ray interacting with medium during the period of EPE; N_A is Avogadro constant; M_A is the Moore mass of the medium.

Accordingly, μ_p/ρ also fully satisfies the following equations:

$$\text{if } hv > 2m_e c^2, \quad \frac{\mu_p}{\rho} = \frac{N_A}{M_A} \sigma_p \propto Zhv \quad (6)$$

$$\text{if } hv > m_e c^2, \quad \frac{\mu_p}{\rho} = \frac{N_A}{M_A} \sigma_p \propto Z \ln(hv) \quad (7)$$

From above theories and formulas, **Figure 2** illustrates region distribution of relative predominate with the three main forms of photon interaction with matter corresponding to the function of photon energy and atomic number [11]. The relationship between the mass attenuation coefficient and the photon energy are shown in **Figure 3** [12].

If the mass attenuation coefficients of the body tissue, such as bone $Z = 12.31$, muscle $Z = 7.64$ and fat $Z = 6.46$, are normalized with the air mass attenuation coefficient, we can acquire the relative mass attenuation coefficients curve which shown in **Figure 4** [13]. **Figure 4** shows PE is a predominant absorption mode when the energy ranges from 10 - 200 keV and named E1 range. As the PE is proportional to the cubic of atomic number and is inversely proportional to the cubic of the photon energy, these leads to the large absorption energy differences among bone, muscle and fat. As the energy increasing, this energy absorption difference rapidly decreases because CE slowly replaces the PE.

As the CE is a predominant energy absorption mode between 200.0 keV - 10.0 MeV energy and named E2 range, the energy absorption differences of these three mediums are almost disappear. The energy absorption curve nearly is a straight line, which shown as the middle section of **Figure 4**, because the CE is almost independent of X-ray energy and atomic number of the medium.

In 10.0 MeV - 100.0 MeV energy domain, which named E3 range, the PE and CE completely disappear and the EPE predominate. Therefore, the mass attenuation coefficients of three types of human tissue are proportional

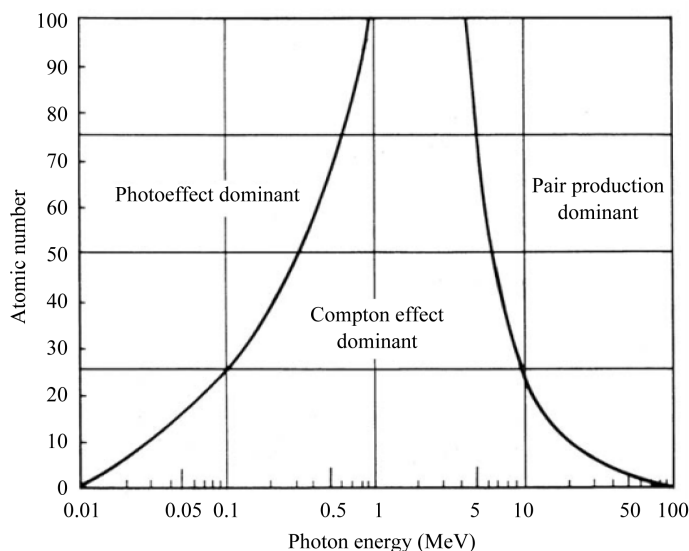


Figure 2. The relation among three interaction forms from photon and medium, photon energy and medium anatomic number.

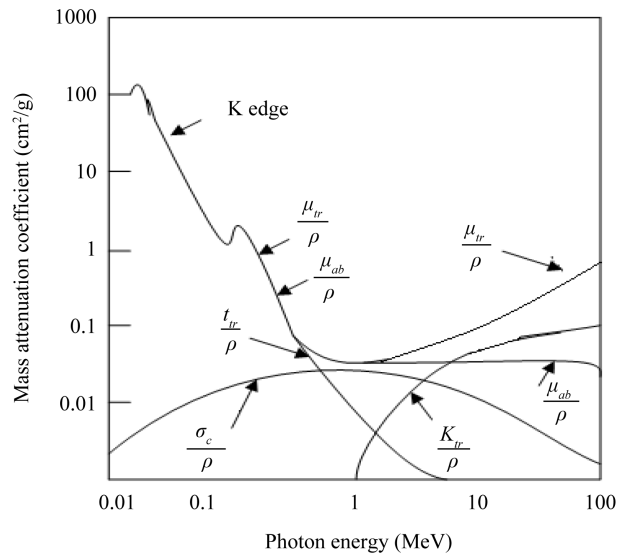


Figure 3. The relationship between mass attenuation coefficient and photon energy.

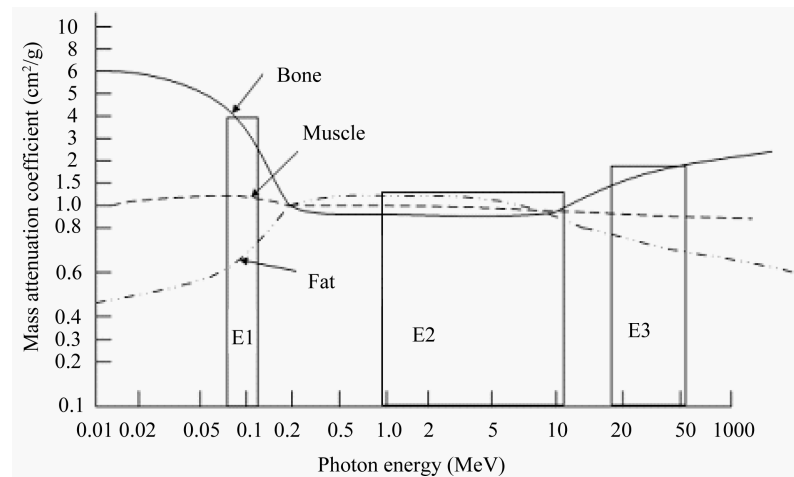


Figure 4. The several of mass attenuation coefficients for bone, muscle and fat with different photon energies. In this figure, E1 represents the Photoelectric Effect becoming a main absorption mode at the ranges of photon energy from 60 keV to 120 keV. E2 means the Compton Effect predominating at the range of photon energy between 1.0 meV to 10 MeV. E3 expresses the Electronic Pair Effect becoming a main absorb mode when photon energy ranges from 20 MeV to 50 MeV.

to the atomic number Z and the photon energy hV and result in increasing bone absorption. The mass attenuation coefficients differences among three human tissues are also significant. When the photon energy is higher than 15 MeV, this phenomenon becomes much more apparent.

In the kV image mode, tube voltage of the X-ray generator ranges from 60 kV to 120 kV; its bremsstrahlung photon energy approximately equals to 40 keV to 80 keV. At this time, the energy range positions in the E1 of **Figure 4** and PE dominates in this region. In addition, at the lower energy value of the energy domain, according to Equation (1), the lower energy leads to the larger cross section area. The detector sensitivity would increase, thereby decreasing noise and increasing the detectability. However, as the energy continue increasing, the cross-section area become decreasing. The detector sensitivity would decrease as well, thereby it leads to increase noise and decrease detectability. Although, there is a decreasing detectability trend within the E1, their differences for the three mediums (bone, muscle and fat) are still huge (as shown in **Figure 3** and **Figure 4**). This is the reason why images quality and the contrast between various tissues and different anatomical structures are both good in

kV image mode.

In the MV image mode, the nominal acceleration potential ranges from 4MV to 15MV and its bremsstrahlung energy approximately equal to 200 keV to 10 MeV. At this moment, the CE majorly dominates in this imaging mode. The mass attenuation coefficient in this region is the lowest (as shown in **Figure 3**) and their difference of various tissues and anatomical structures is almost zero (as shown in **Figure 4**). In addition, as MV energy increases, the exit dose and detector sensitivity would decrease, thereby lead to increase noise and lower detectability. Consequently, the image quality and contrast or resolving capability among these tissues and anatomical structures are the lowest.

According to the above-mentioned theory and analysis, HMV locates in E3 range of **Figure 4**. EPE dominates in this region. In comparison, the mass absorption coefficient is larger and the difference of X-ray absorption coefficient among three tissues (bone, muscle and fat) is much more considerable than the difference has been found in the MV imaging mode (see **Figure 3**). In addition, as HMV energy increases, the exit dose and detector sensitivity would increase, thereby decreasing noise and increasing detectability. So this mode not only offers better images quality, but also gains better contrast or resolving capability between tissues and anatomical structures than conventional MV imaging mode.

3. Experiment

All experiments have been done by using The linear accelerator (LA 45, Top Grade Healthcare, Beijing, China), shown in **Figure 5**. The incident X-ray energy that used for approving previous theoretical statements was 10 MV, 25 MV and 45 MV bremsstrahlung, which was equivalent to 8 MeV, 13 MeV and 30 MeV X-ray energy respectively [14].

PekinElmer, a company in Germany, provided X-ray imaging system. The X-ray flat panel detector used in experiments was an indirect conversion type and consisted of amorphous silicon. The CsI (TI) scintillator (Pekin-Elmer, Germany) with XIS3.2.0.67 image acquisition and analyzing software also included in the panel. The series number of the X-ray panel detector is XRD 1640 AN19 CS. The flat panel's physical dimension is "16 × 16" with the precise of 200 μm (nominal spatial resolution 2.5 lp/mm). The original projection acquired from flat panel was 16 bit (or 65,000 grayscale) and had a resolution of 1024 × 1024 pixels.

The image detector panel (**Figure 6(a)**) placed under the treatment head of the LA45 accelerator. The distance between flat panel's surface and X-ray source was 1480 cm. The center of the medium (phantom or patient) that need to be scanned located at isocenter of LA45. The dose of single expose was 2cGy each time, took 600 ms acquisition time for collecting three frame images and chose the best quality one.

The phantom used in the experiments was the Catphan 500 (**Figure 6(b)**) cylinder phantom (acquired from The Phantom Laboratory, NewYork, USA), which was mainly used for evaluating the scanning performance of CT or CTBT as consisting of several material modules in different density and computed tomography (CT) value (range from -1000 Hu, -200 Hu, -100 Hu, -35 Hu, 120 Hu, 340 Hu, 990 Hu) [15]. In this study, the phantom used for evaluating image quality of FPD with different X-Ray's energy irradiation (10 MV, 25 MV and 45 MV), where 10 MV stands for MV imaging mode and 45 MV stands for HMV imaging mode. Based on this experiment's result, a real patient's abdomen was also be scanned with the same method. All images were acquired by using screenshot in high-resolution medical displayer and were processed with Paint tool from Windows software.



Figure 5. The LA45 linear accelerator used in this experiment.

4. Results

The images of the Catphan 500 phantom from 10 MV, 25 MV and 45 MV with 2cGy high energy bremsstrahlung irradiation are respectively shown in **Figures 7(a)-(c)**. **Figure 8(a)** is a verification image that was acquired from the world famous accelerator with 6 MV X-ray IGRT system of a patient's abdomen image. **Figures 8(b)-(d)** are abdomen images of the same patient with 10, 25, 45 MV for 2cGy high energy bremsstrahlung irradiation, respectively.

5. Discussions

Obviously, the image quality and the resolution of 45 MV bremsstrahlung irradiation on either Catphan 500 phantom or patients has better resolution than the image acquired of 25 MV bremsstrahlung. The latter is also superior to each of image acquired from 10 MV and 6 MV, respectively. This result conformed to the statements that derived from theoretically analyzing in previous sections. The advantages of using HMV image mode were more apparent than applying conventional kV and MV imaging mode. If using high-resolution medical displayer directly analyzes these images, the advantages of HMV would be much more apparent.

Theoretical and experimental results show that HMV image mode not only improves the image quality, but also has good resolving capability to identify tissues components. As the detector placed below treatment head and shares the same source of treatment, HMV imaging mode prevents drawbacks of position verification from both kV and MV level imaging mode as well as keeps their advantages.

6. Conclusion

In conclusion, HMV is a good imaging verification mode in radiotherapy; it will play a sensible role in radio-

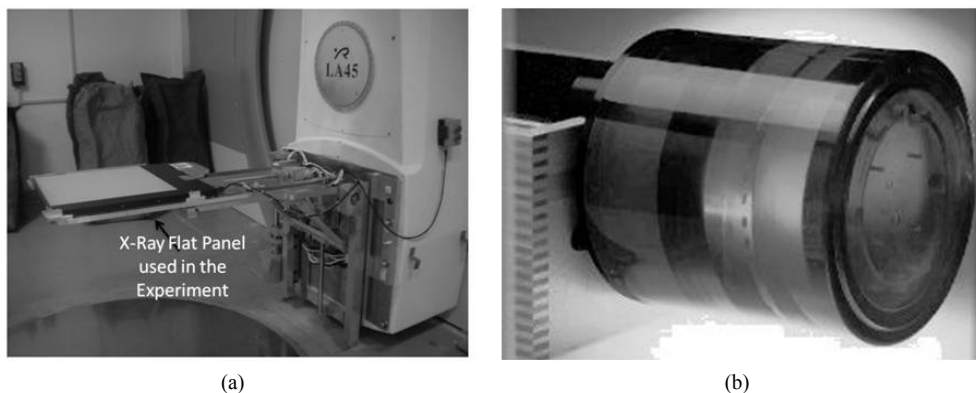


Figure 6. (a) X-ray flat panel detector used in this experiment; (b) Catphan 500 cylinder phantom.

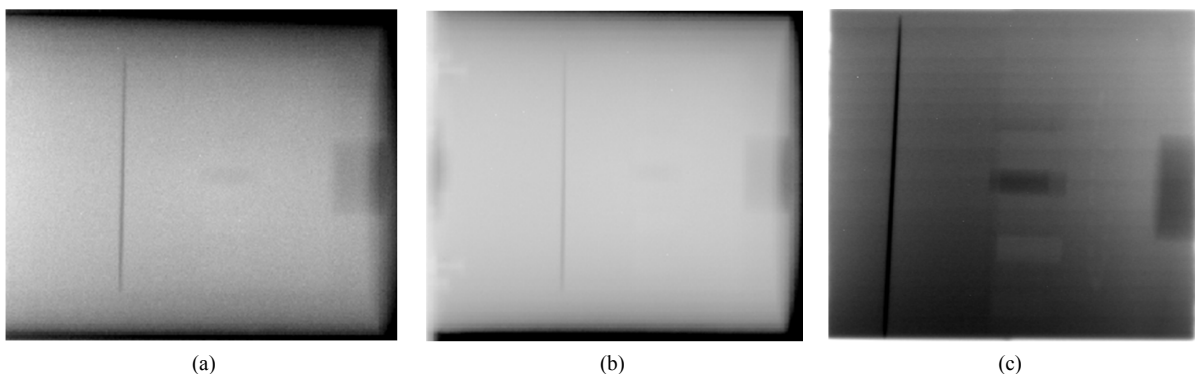


Figure 7. Comparison with different bremsstrahlung energies irradiated on the Catphan 500 phantom. The phantom is irradiated by 10 MV bremsstrahlung (a), 25 MV bremsstrahlung (b) and 45 MV bremsstrahlung (c), respectively. The main difference of these images is also pointed.

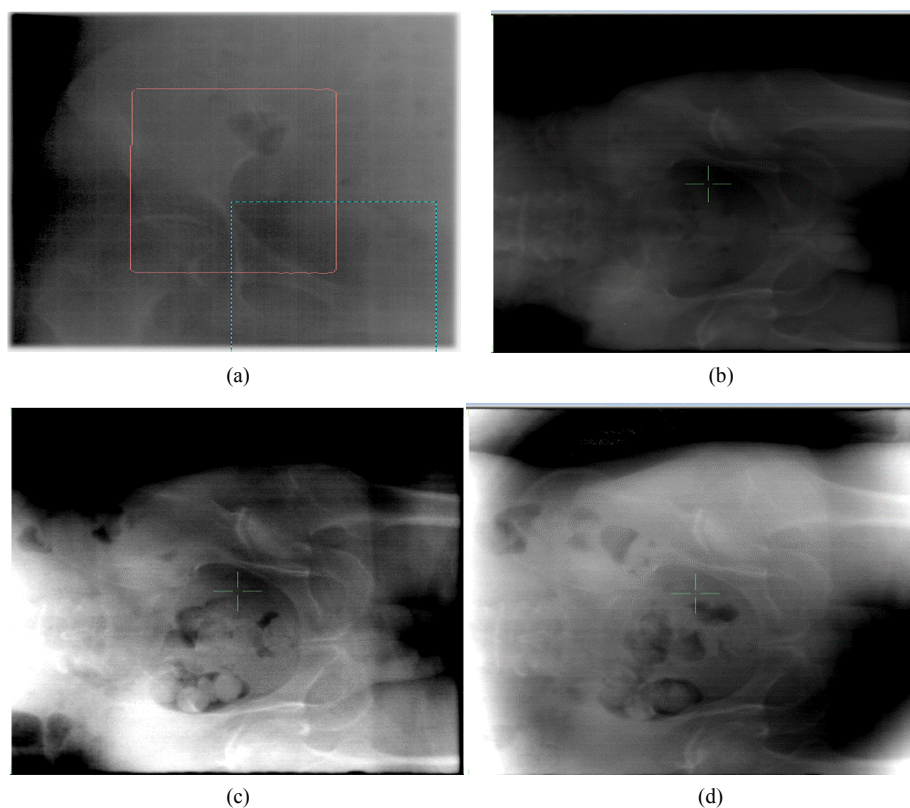


Figure 8. Abdomen images of the same patient from various bremsstrahlung X-ray energies compare to conventional 6 MV X-ray IGRT. (a) 6 MV radiation image from the world famous accelerator; (b) abdomen was irradiated with 10 MV bremsstrahlung; (c) abdomen was irradiated with 25 MV bremsstrahlung and (d) abdomen was irradiated with 45 MV bremsstrahlung.

therapy position verification.

References

- [1] Hurkmans, C.W., Cho, B.C., Damen, E., Zijp, L. and Mijnheer, B.J. (2002) Reduction of Cardiac and Lung Complication Probabilities after Breast Irradiating Using Conformal Radiotherapy with or without Intensity Modulation. *Radiation Oncology*, **22**, 163-171. [http://dx.doi.org/10.1016/S0167-8140\(01\)00473-X](http://dx.doi.org/10.1016/S0167-8140(01)00473-X)
- [2] Jacob, R., Hanlon, A.L., Horwitz, E.M., Movsas, B., Uzzo, R.G. and Pollack, A. (2004) The Relationship of Increasing Radiotherapy Dose to Reduced Distant Metastases and Mortality in Men with Prostate Cancer. *Cancer*, **100**, 538-543. <http://dx.doi.org/10.1002/cncr.11927>
- [3] Chen, J., Morin, O., Aubin, M., Bucci, M.K., Chuang, C.F. and Pouliot, J. (2006) Dose Guided Radiation Therapy with Megavoltage Cone Beam CT. *The British Journal of Radiology*, **79**, S87-S98. <http://dx.doi.org/10.1259/bjr/60612178>
- [4] Jaffray, D.A., Siewerdsen, J.H., Wong, J.W. and Martinez, A.A. (2002) Flat Panel Cone-Beam Computed Tomography for Imaging Guided Radiation Therapy. *International Journal of Radiation Oncology, Biology, Physics*, **53**, 1337-1449. [http://dx.doi.org/10.1016/S0360-3016\(02\)02884-5](http://dx.doi.org/10.1016/S0360-3016(02)02884-5)
- [5] Pouliot, J., Bani-Hashemi, A., Chen, J., Svator, M., Ghelmansarai, F., Mitschke, M. and Xia, P. (2005) Low-Dose Megavoltage Cone-Beam CT for Radiation Therapy. *International Journal of Radiation Oncology, Biology, Physics*, **61**, 552-560. <http://dx.doi.org/10.1016/j.ijrobp.2004.10.011>
- [6] Groh, B.A., Siewerdsen, J.H. and Drake, D.G. (2002) A Performance Comparison of Flat-Panel Imager-Based MV and kV Cone-Beam CT. *Medical Physics*, **29**, 967-975. <http://dx.doi.org/10.1118/1.1477234>
- [7] Ruchala, K.J., Olivera, G.H., Schloesser, E.A. and Mackie, T.R. (1999) Megavoltage CT on a Tomotherapy System. *Physics in Medicine and Biology*, **44**, 2597-2621. <http://dx.doi.org/10.1088/0031-9155/44/10/316>
- [8] (2015) Personal Conversation with Experts at the American Association of Physicists in Medicine (AAPM).

- [9] Murphy, M.J., Balter, J., Balter, S., Bencomo, J.A., Das, I.J., Jiang, S.B., Ma, C.M., Olivera, G.H., Rodebaugh, R.F., Shirato, H. and Yin, F.F. (2007) The Management of Imaging Dose during Image-Guided Radiotherapy: Report of the AAPM Task Group 75. *Medical Physics*, **34**, 4041-4060. <http://dx.doi.org/10.1118/1.2775667>
- [10] Liu, L., Antonuk, L.E., El-Mohri, Y., Zhao, Q.H. and Jiang, H. (2015) Theoretical Investigation of the Design and Performance of a Dual Energy (kV and MV) Radiotherapy Imager. *Medical Physics*, **42**, 2072-2084. <http://dx.doi.org/10.1118/1.4915120>
- [11] Thilmann, C., Nill, S., Tücking, T., Hoss, A., Hesse, B., Dietrich, L., Bendl, R., Rhein, B., Häring, P., Thieke, C., Oelfke, U., Debus, J. and Huber, P. (2006) Correction of Patient Positioning Errors Based on In-Line Cone Beam CTs: Clinical Implementation and First Experiences. *Radiation Oncology*, **24**, 1-16.
- [12] Podgorsak, E.B. (2005) *Radiation Oncology Physics: A Handbook for Teachers and Students*. International Atomic Energy Agency, Vienna.
- [13] Hu, Y.M. (1999) *The Tumor Radiation Physics*. Atomic Energy Press, Beijing.
- [14] Zhang, Q.S., Zhang, M. and Wu, X.Y. (2005) Research on Radiation Quality and Scanning Beam Characteristics of Medical Electron Cyclotron. *Chinese Journal of Medical Physics*, **22**, 376-378.
- [15] Guan, H.Q. and Dong, H. (2009) Dose Calculation Accuracy Using Cone-Beam CT for Pelvic Adaptive Radiotherapy. *Physics in Medicine and Biology*, **54**, 6239-6250. <http://dx.doi.org/10.1088/0031-9155/54/20/013>